The density and the average energy of the fast alpha particles in the D-He3 reaction are found as
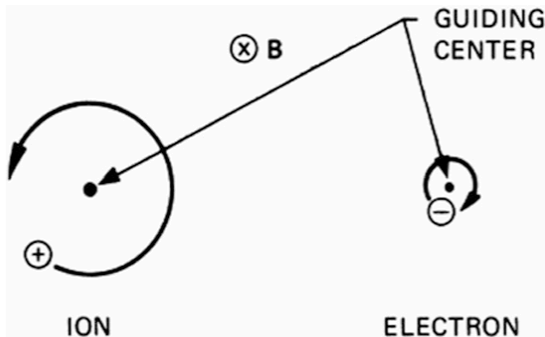Variables: nf = CDCHe3n2 i vDHe3 f

$E\frac{1}{4}0$ In this case, a charged particle has a simple cyclotron gyration. The equation of motion is mdv dt ¼
qv B and the direction of plasma structures-particles B (B¼B ^ z)

The chemical variable-structures are for example;
E to lie in the x–z plane so that Ey¼0. As before, the z component of velocity is unrelated to the
transverse components and can be treated separately. The equation of motion is now mdv dt ¼ q Ev B ð Þ
ð2:8Þ whose z component is or q dvz dt ¼ m Ez.

General formula: E þ v B¼0
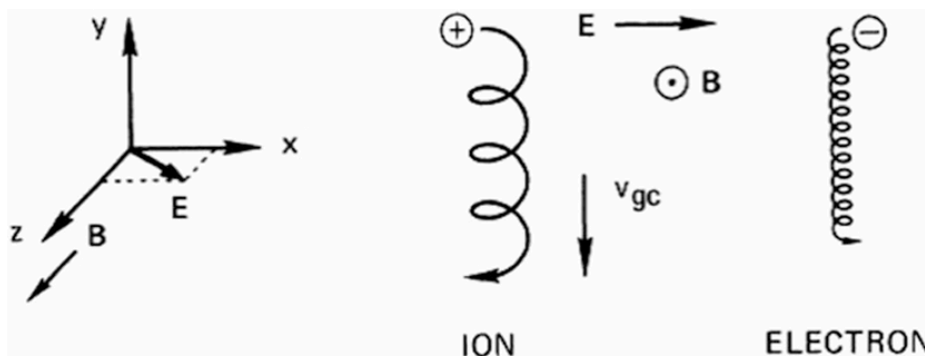
E B ¼ B v B ð Þ¼vB2 Bv B

The transverse components of this equation are

v⊥gc ¼ E B=B2 vE ð Þ ð2:14Þ ð2:15Þ

We can define this to be vE, the electric field drift of the guiding center. In magnitude, this drift is E V=m
vE ¼ ð Þ B B tesla m sec. A negative electron gyrates in the opposite direction but also gains energy in the
opposite direction; it ends up drifting in the same direction as an ion. For particles of the same velocity
but different mass, the lighter one will have smaller rL and hence drift less per cycle. However, its

gyration frequency is also larger, and the two effects cancel. Two particles of the same mass but different energy would have the same ωc. The slower one will have smaller rL and hence gain less energy from E in a half cycle. In the gravitational Field The foregoing result can be applied to other forces by replacing qE in the equation of motion by a general force F.

The guiding center drift caused by F is then vf ¼1 q F B B2 In particular, if F is the force of gravity mg, there is a drift vg ¼m q g B B2 ð2:17Þ ð2:18Þ

This is similar to the drift vE in that it is perpendicular to both the force and B, but it differs in one important respect.

Materials: Liquid Infiltration Carbonization Liquid infiltration carbonization is the traditional method used to prepare graphite materials and has become an important technique to prepare C/C composites. A flowchart of this process is shown in Fig. 5.1. Through repeated infiltration:
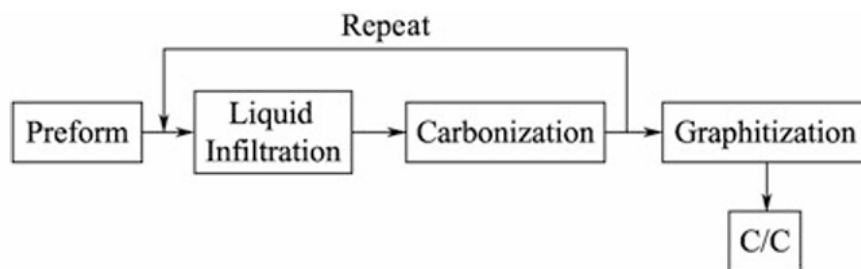
Unneutralized electron beam has density ne¼1014 m 3 and radius a¼1cm and flows along a 2-T magnetic field. If B is in the +z direction and E is the electrostatic field due to the beam's charge, calculate the magnitude and direction of the E B drift at r¼a :
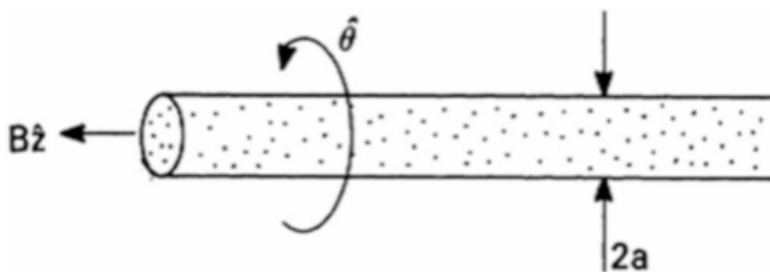
Structural plasma: The gradient in jBj causes the Larmor radius to be larger at the bottom of the orbit than at the top, and this should lead to a drift, in opposite directions for ions and electrons, perpendicular to both B and ∇B. The drift velocity should obviously be proportional to rL/L and to v⊥. Consider the Lorentz force F¼qv B, averaged over a gyration. Clearly, Fx ¼ 0; since the particle spends as much time moving up as down. We wish to calculateFy; in an approximate fashion, by using the undisturbed orbit of the particle to find the average.
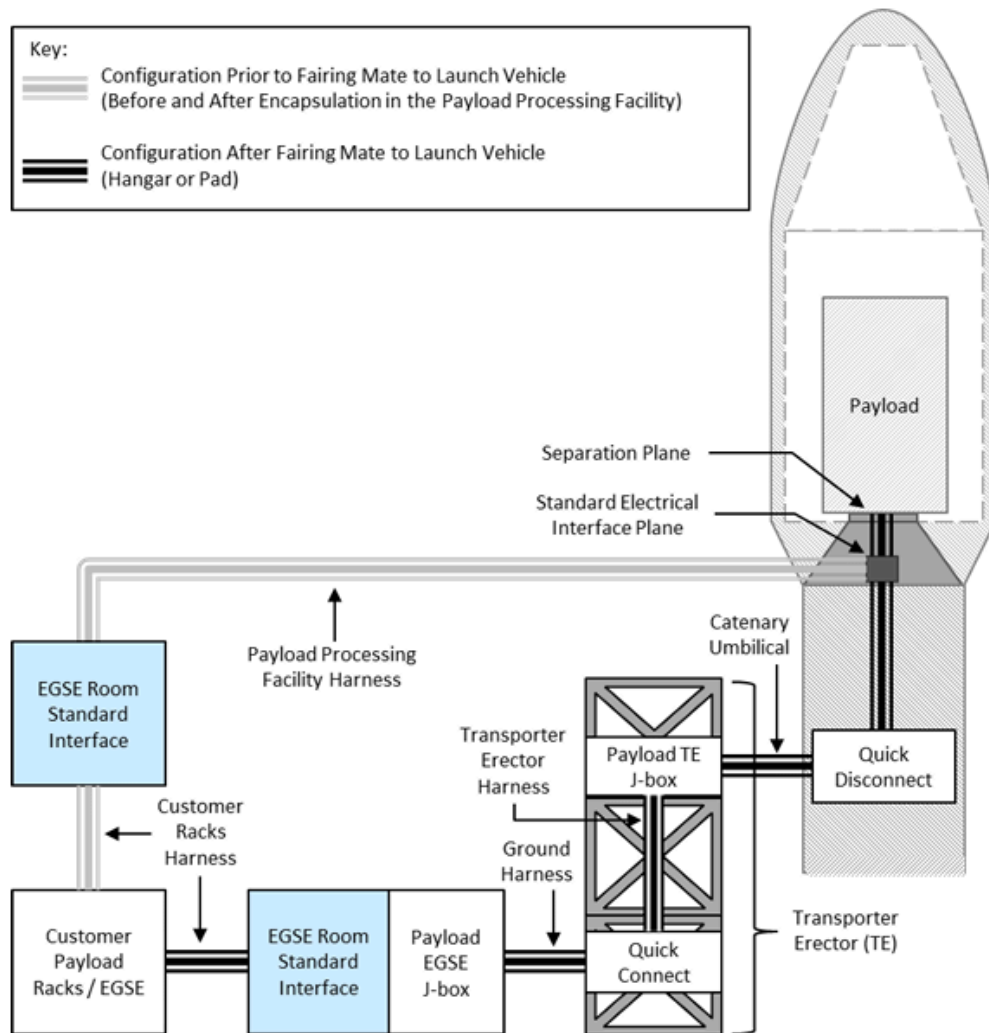
Figure 5-1: On-pad electrical interfaces

Mechanical interface & cooling structural particles in plasma fusion variables: B ¼ B0þ r ▽ ð ÞBþ Bz ¼ B0 þy ∂Bz=∂y ð Þþ ð2:21Þ This expansion of course requires rL/L 1, where L is the scale length of ∂Bz/∂y.

Variables-equation is in this case the center drift velocity is then vgc ¼1 q 1 F B B2 ¼ q Fy B j j ^ x ¼ v⊥rL B 1 2 ∂B ∂y ^ x ð2:23Þ.

the lines of force to be curved with a constant radius of curvature Rc, and we take jBj to be constant Such a field does not obey Maxwell's equations in a vacuum, so in practice the grad-B drift will always be added to the effect derived here. A guiding center drift arises from the centrifugal force felt by the particles as they move along the field lines in their thermal motion.

If v^2_k denotes the average square of the component of random velocity along B, the average centrifugal force is $F_{cf} = mv^2_k R_c \hat{r} = mv^2_k R$ According to Eq. (2.17), this gives rise to a drift $v_R = \frac{1}{q} \frac{F_{cf} \times B}{B^2} = \frac{c}{R^2_c} \frac{mv^2_k}{qB^2} \frac{R_c \times B}{R^2_c}$ (2.25) (2.26)

1 Vehicle integration hangar
2 Hangar annex
3 Launch pad
4 Pad customer room

Space Launch Complex 40
Launch Pad
Large Processing Facility
Hangar X
SpaceX Launch Control
Cape Canaveral
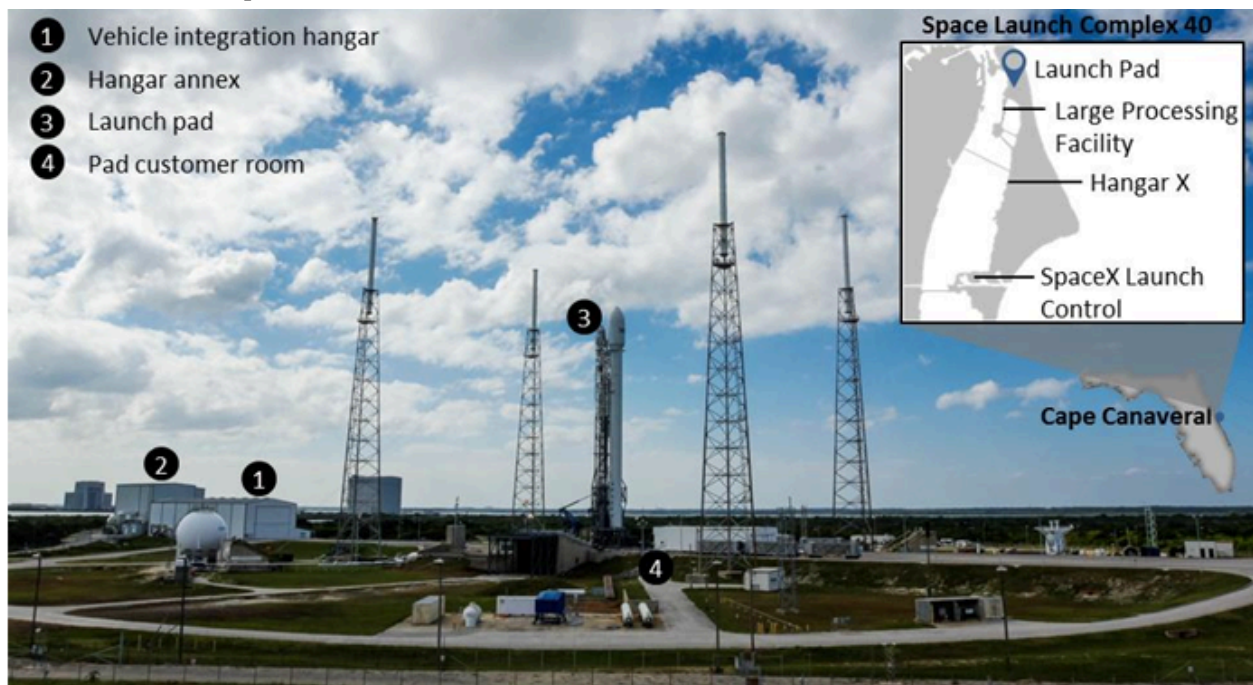
$\nabla B \| B$: Magnetic Mirrors are a magnetic field which is pointed primarily in the z direction and whose magnitude varies in the z direction. Let the field be axisymmetric, with $B_\theta = 0$ and $\partial/\partial\theta = 0$. Since the lines of force converge and diverge, there is necessarily a component B_r. A magnetic field trapping particles structural variables or parameters can be in a technical draw:
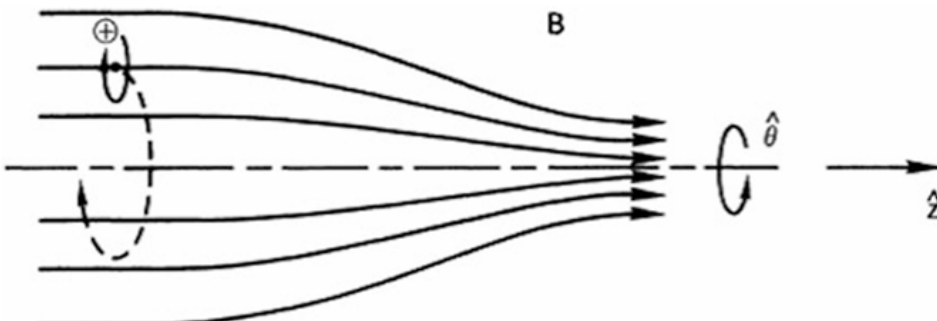
The invariance of μ is the basis for one of the primary schemes for plasma confinement: the magnetic mirror. As a particle moves from a weak-field region to a strong-field region in the course of its thermal motion, it sees an increasing B, and therefore its $v_\perp$ must increase in order to keep μ constant. Since its total energy must remain constant, v_k must necessarily decrease. If B is high enough in the "throat" of the mirror, v_k eventually becomes zero; and the particle is "reflected" back to the weak-field region. It is, of course, the force F_k which causes the reflection. The nonuniform field of a simple pair of coils forms two magnetic mirrors between which a plasma can be trapped.This effect works on both ions and electrons.

The trapping is not perfect, however. For instance, a particle with $v_\perp = 0$ will have no magnetic moment and will not feel any force along B.

A particle with small $v_\perp = v_\parallel$ at the midplane ($B = B_0$) will also escape if the maximum field B_m is not large enough. For given B_0 and B_m, which particles will escape? A particle with $v_\perp = v_{\perp 0}$ and $v_\parallel = v_{\parallel 0}$ at the midplane will have $v_\perp = v'_\perp$ and $v_\parallel = 0$ at its turning point. Let the field be B' there. Then the invariance of μ yields $\frac{1}{2} m v_{\perp 0}^2 = B_0 =$

Conservation of energy requires $\frac{1}{2} m v_{0\perp}^2 = B_0$
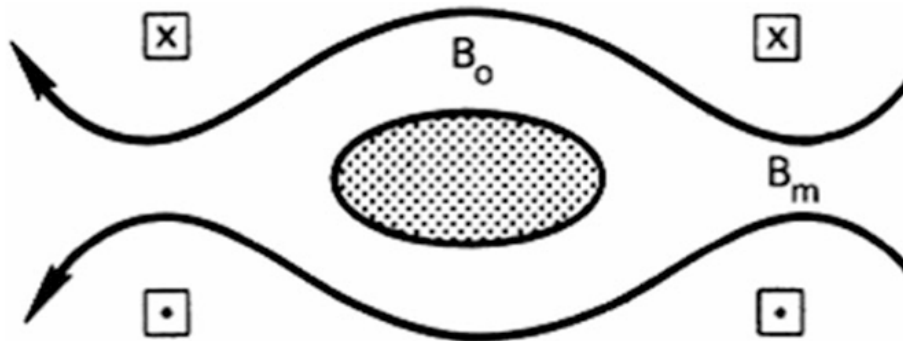
The Structure and Propulsion The first-stage propellant tank walls of the Falcon vehicles are made from an aluminum lithium alloy. Tanks are manufactured using friction stir welding—the highest strength and most reliable welding technique available. Figure 2-1 Falcon 9 Overview On the first stage of the Falcon 9, an insulated common dome separates the LOX and RP-1 tanks, and an insulated transfer tube carries LOX through the center of the RP-1 tank to the engine section. Four grid fins near the top of the first stage along with four deployable legs are nominally flown at the base of the first stage to support recovery operations. The second-stage tank for Falcon vehicles is a shorter version of the first-stage tank and uses most of the same materials, construction, tooling and manufacturing techniques as the first-stage tank. A single Merlin Vacuum (MVac) engine powers the second stage, using a fixed 165:1 expansion nozzle. For added reliability of restart, the engine contains dual redundant triethylaluminum-triethylborane (TEA-TEB) pyrophoric igniters. In addition, the second stage contains a cold nitrogen gas (GN2) attitude control system (ACS) for pointing and roll control. The GN2 ACS is more reliable and produces less contamination than a propellant-based reaction control system.

```
Table 2-1: Falcon 9 Dimensions and Characteristics

Characteristic
First Stage
Structure
Second Stage

Height
70 m (229 ft) (including both stages, interstage, and fairing)
```

Diameter
3.66 m (12 ft)

Type
3.66 m (12 ft)
LOX tank – monocoque
Fuel tank – skin and stringer

Material
LOX tank – monocoque
Fuel tanks – skin and stringer
Aluminum lithium skin; aluminum domes

Propulsion
Engine Type
Liquid, gas generator

Engine Designation
Merlin 1D (M1D)

Engine Designer
MVac
SpaceX

Engine Manufacturer
SpaceX

Number of Engines
First Stage: 9
Second Stage: 1

Propellant
Liquid oxygen/kerosene (RP-1)

Thrust (Stage Total)
Sea Level: 6,804 kN (1,530,000 lbf)
Vacuum: 934 kN (210,000 lbf)

Propellant Feed System
Turbopump

Throttle Capability
Yes (170,000 lbf to 119,000 lbf sea level)

Restart Capability
Yes (210,000 lbf to 81,000 lbf)

Tank Pressurization
Yes
Heated helium

```
Ascent Attitude Control
Pitch, Yaw: Gimbaled engines

Coast Attitude Control
Gimbaled engine/nitrogen gas thrusters
```

The first and second stages are mated by mechanical latches at three points between the top of the interstage and the base of the second-stage fuel tank. After the first-stage engine shut down, a high pressure helium circuit is used to release the latches via redundant actuators. The helium system also preloads three pneumatic pushers, which provide positive-force stage separation after latch release. For added reliability, a redundant center pusher attached to the first stage is designed to dramatically decrease the probability of re-contact between the stages following separation. The two halves of the fairing are fastened by mechanical latches along the fairing vertical seam. To deploy the fairing, a high-pressure helium circuit releases the latches, and four pneumatic pushers facilitate positive-force deployment of the two halves. The use of all-pneumatic separation systems provides a benign shock environment, allows acceptance and preflight testing of the actual separation system hardware, and minimizes debris created during the separation event.

Avionics, and Guidance, Navigation and Control Falcon avionics feature a three-string, fault-tolerant architecture that has been designed to human-rating requirements. Avionics include flight computers, Global Positioning System (GPS) receivers, inertial measurement units, SpaceX-designed and manufactured controllers for vehicle control (propulsion, valve, pressurization, separation and payload interfaces), a network backbone, S-band transmitters and a C-band transponder for range safety tracking. The S-band transmitters are used to transmit telemetry and video to the ground, from both the first and second stages, even after stage separation. Our launch vehicles are equipped with a flight termination system to limit the potential damage caused by a launch vehicle malfunction. The system terminates the flight of the vehicle either when commanded by the range mission flight control officer or automatically in the case of premature stage separation. 2.5 Coordinate Frame Falcon vehicles use a right-hand X-Y-Z coordinate frame centered 440.69 cm (173.5 in.) aft of the first stage radial engine gimbal, with +X aligned with the vehicle long axis and +Z opposite the transporter erector strongback.

X is the roll axis, Y is the pitch axis, and Z is the yaw axis. Additional coordinate frames may be defined with reference to the payload interface for specific missions. Plasma: The magnetic mirror was first proposed by Enrico Fermi as a mechanism for the acceleration of cosmic rays. Protons bouncing between

magnetic mirrors approaching each other at high velocity could gain energy at each bounce:
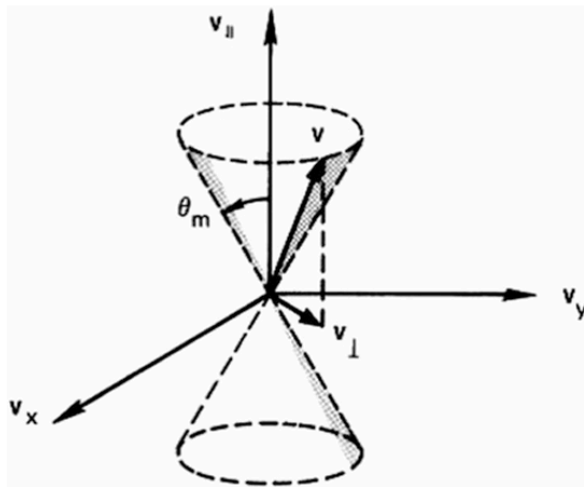
Non Uniform E Field Now Let the magnetic field be uniform and the electric field be non uniform. For simplicity, we assume E to be in the x direction and to vary sinusoidally in the x direction (Fig. 2.11): E E0 cos kx ð Þ^ x ð2:47Þ

This magnetic mirror field distribution has a wavelength $\lambda \frac{1}{4} 2\pi/k$ and is the result of a sinusoidal distribution of charges, which we need not specify. In practice, such a charge distribution can arise in a plasma during a wave motion. The equation of motion is mdv=dt ð Þ¼qEx ð Þþv B.

Composites summary:
Resin Infiltration Carbonization The resin used in liquid infiltration carbonization must be selected carefully. The resin must meet the following conditions [1, 6]:

1. Appropriate viscosity, good flowability, and easily infiltrates into the preform;

2. High carbon yields after carbonization to increase infiltration efficiency and gives high bulk density; 3. Low volume shrinkage during infiltration, solidification, and carbonization processes to decrease damage to fibers.

Staple thermoplastic resins used to prepare C/C composites are polyetheretherketone (PEEK) and polyetherimide (PEI). Although using these resins can efficiently decrease the number of infiltration times, pressure is needed to increase the efficiency during solidification. Most resins used in this industry are thermosetting ones, such as phenolic, ethoxyline, furan, furyl ketone, acetylenic, and polyimide. Most thermosetting resins readily cross-link at relatively low temperature to form thermosetting, infusible, and vitreous solids. The resin carbon after carbonization is difficult to graphitize; however, resin carbon can also be graphitized under stress at high temperature and pressure.
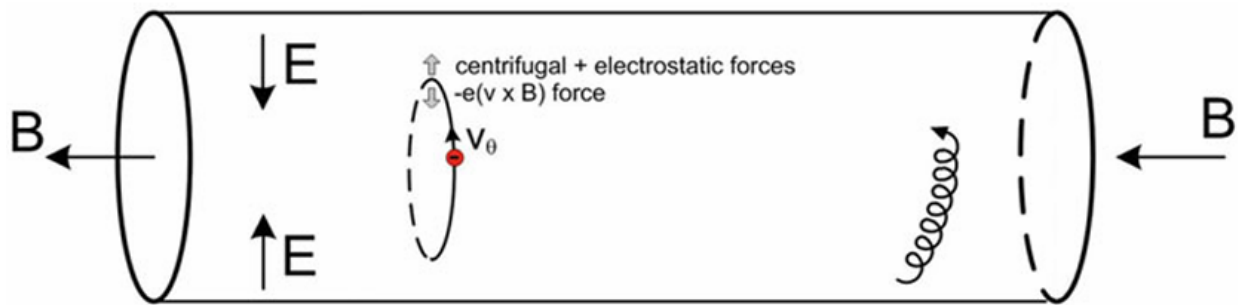
Variables: ωr is independent of radius, we see that such a pure electron plasma rotates as a solid body. When $\omega 2 \, p = \omega 2 \, c > \frac{1}{2}$, there is no solution; otherwise, there are two solutions. For $2\omega 2 \, p = \omega 2 \, c \ll 1$, expanding the square root yields the frequencies $\omega r \, \omega c$, and the lower frequency $\omega r \, \omega 2 \, p = 2\omega c \, \omega D$: ð9:5Þ Called the diocotron frequency, ωD has an orbit like the one at the right in Fig. 9.1. With appropriate modifications, these equations can also describe pure ion plasmas.

Solid, Ultra-Cold Plasmas By freezing the plasma in an ion trap to sub-Kelvin temperatures, it is possible to create liquid and solid plasmas. As the thermal motions of the particles decrease, their thermal energies become comparable to the Coulomb energy Wc between particles. This condition can be quantified by defining a coupling parameter Γ, the ratio between the average Wc and KT. Two singly charged particles separated by a distance a have a Coulomb energy e2/a.

Hence $\Gamma \, \frac{1}{4} e2 = aKT$: The Pair-ion Plasmas parameters that a plasma with equal masses would behave quite differently from a normal plasma with slow ions immersed in a sea of fast electrons. Though it is possible to make a positronium plasma, the recombination rate is so fast that there is no time to do experiments. Fullerenes, stable molecules of 60 carbon atoms arranged in a hollow sphere, move and recombine slowly because of the large mass. It is thus possible to produce a long-lived pair-ion plasma with C60. In Fig. 9.5, neutral C60 is injected from an oven. A ring of fast electrons up to 150 eV driven through the C60 forms Cþ 60 ions by ionization and C60 ions by attachment. A magnetic field confines the electrons but allows the heavy ions to diffuse into the center to form a fullerene pair-ion plasma. The plasma then passes through a hole into a chamber for experimentation. Consider a singly charged pair-ion plasma with a common mass M and temperature KT. The equations of motion for the ions of charge + or are Mn0 dv dt $\frac{1}{4}$ n0E ∇p:

 Dust grains have sizes from tens of nanometers to hundreds of microns. Since electrons impinge on them much more often than ions do, the grains will have a negative surface potential Vs. Consider a spherical grain of radius a and charge q<0. The capacitance of the sphere (with distant walls) is C $\frac{1}{4}4\pi\varepsilon0a$: The surface charge q is then q $\frac{1}{4}$CVs $\frac{1}{4}4\pi\varepsilon0aVs$: ð9:16Þ ð9:17Þ The value of either q or Vs depends on the Debye length λD in the background plasma. If λD is a, the grain is a small, isolated particle like a spherical Langmuir.
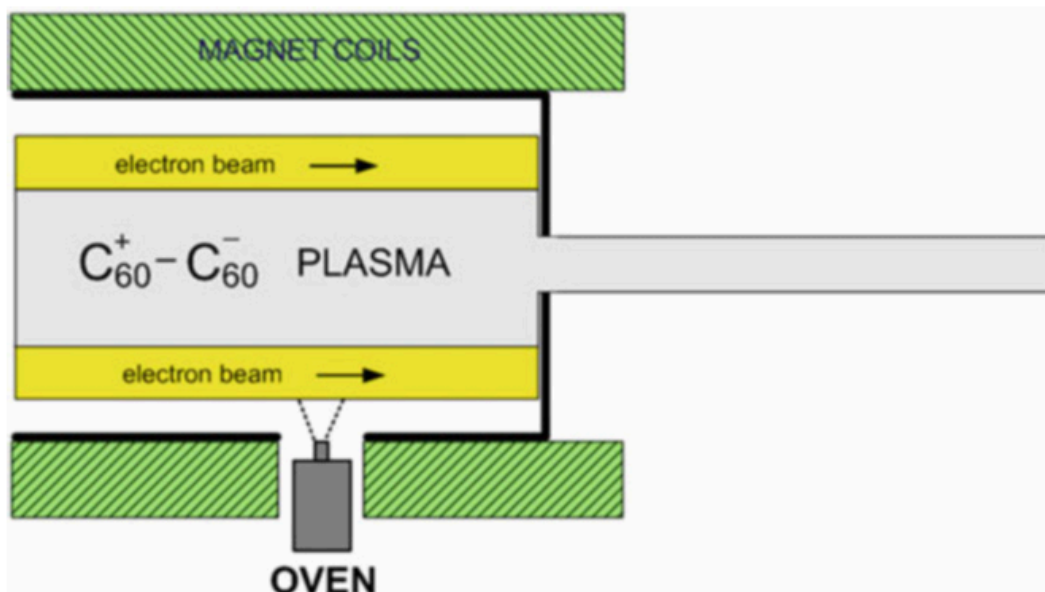
Variables-structure:

The Dust Acoustic Waves The dust acoustic wave is a very low-frequency, longitudinal compressional wave involving the motions of the dust particles. Because the heavy dust moves more slowly than the ions and electrons, the latter have time to relax into Maxwellian distributions:

1. ne ¼ ne0 exp eφ=KTe ð Þ¼ne0 1þeφ=KTeþ

2. ð Þ, ne ni ¼ ni0 exp eφ=KTi ð Þ¼ni 0 1 eφ=KTiþ.

3. 1 ¼ne0 eφ=KTe ð Þ ð Þ, ni 1 ¼ni0 eφ=KTi ð Þ

Variables-expressions-python:

```
Fluid Motion Equation (Including Collisions)

For any species, the equation of motion is:
mndv/dt = mn(∂v/∂t) + v∇(v) = enE - ∇p - mnvv

- The term "enE" represents the force due to an electric field.
- "∇p" accounts for pressure gradients within the fluid.
- The averaging process ensures Eq. (5.5) remains valid.
- In a **steady-state plasma**, ∂v/∂t = 0, meaning fluid elements do
not move into regions
  with different E or ∇p within a collision time.

Setting dv/dt = 0 leads to:
v = (1 / mnv) * (enE - KT∇n)
```
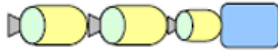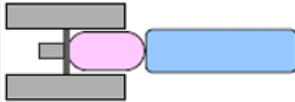
```
        = e / (mvE) - (KT / mv) * ∇(n/n)
```

Key Coefficients:
- **Mobility**: μ = |q| / mv
- **Diffusion Coefficient**: D = KT / mv

These coefficients determine how charged particles move through the plasma,
describing their **response to electric fields** and **thermal diffusion**.

100 mT IMLEO System	Specific Impulse (seconds)	Payload from 400 km LEO to 1-sol Mars orbit (mT)	Total Flight Time (months)
Chemical	450	29	9
Nuclear Thermal	925	44	9
1 MW Solar Electric	5000	48 – 58 (α = 20, α = 10)	27

Velocities in plasma are Γ_i and Γ_e were not equal, a serious charge imbalance would soon arise. If the plasma is much larger than a Debye length, it must be quasineutral; and one would expect that the rates of diffusion of ions and electrons would somehow adjust themselves so that the two species leave at the same rate. How this happens is easy to see. The electrons, being lighter, have higher thermal velocities and tend to leave the plasma first. A positive charge is left behind, and an electric field is set up of such a polarity as to retard the loss of electrons and accelerate the loss of ions. The required E field is found by setting Γ_i ¼Γ_e¼Γ.

PYTHON

```
### Plasma Fluid Motion & Transport Properties

Plasma is a highly dynamic, electrically charged fluid where
particles interact
through electromagnetic forces and collisions. Understanding **plasma
transport**
involves analyzing how ions and electrons move under different
influences.

#### General Fluid Equation of Motion:

mndv/dt = enE - ∇p - mnvv

Where:
- **m** → Mass of the charged species
- **n** → Number density of species
- **dv/dt** → Convective derivative (fluid acceleration)
- **E** → Electric field applied to plasma
- **∇p** → Pressure gradient affecting particle flow
- **mnvv** → Collision term representing momentum exchange between
species

Assuming **steady-state conditions** (∂v/∂t = 0), the equation
simplifies to:

v = (1 / mnv) * (enE - KT∇n)

This relationship highlights two primary factors:
1. **Mobility (µ)** → Response of charged particles to an electric
field
    µ = |q| / mv
2. **Diffusion Coefficient (D)** → Spread of particles due to
temperature gradients
    D = KT / mv

---

### **Mobility and Diffusion in Plasma Transport**

#### **Mobility (µ) – How Particles Respond to Fields**
Mobility **quantifies how quickly charged species move under an
electric field**,
depending on mass, charge, and collision frequency.
- **Low-mass particles (electrons)** → Higher mobility, rapid
response
- **High-mass ions** → Lower mobility, slower reaction
- **High collision rates** → Reduce mobility by disrupting particle
acceleration
```

When mobility is **high**charged species accelerate efficiently,
leading to rapid flow.
In **low-mobility conditions**external forces struggle to drive
plasma movement.

Applications of mobility:
- **Plasma thrusters** → Ion propulsion in spacecraft
- **Fusion reactors** → Maintaining plasma confinement
- **Semiconductor processing** → Controlling ionized particles

---

Diffusion (D) – Random Motion from Thermal Effects
Diffusion describes how particles spread **due to temperature
variations** rather than
direct electromagnetic forces.
- **High-temperature plasma** → More rapid diffusion
- **Dense plasma** → Slower diffusion due to frequent collisions

In weakly ionized plasmas, diffusion often **dominates** transport,
meaning particles
move **without a significant electric field influence**.

Applications of diffusion:
- **Magnetosphere studies** → Understanding charged particle
dispersion
- **Controlled fusion** → Managing energy losses
- **Space plasma physics** → Investigating solar wind interactions

---

Steady-State Plasma & Collisional Effects
In many plasma applications, assuming a **steady-state condition**
simplifies analysis:
$\partial v/\partial t = 0$

- **Low collision plasma** → Transport dominated by electromagnetic
forces
- **High collision plasma** → Transport dominated by diffusion &
thermal gradients

In cases where **fluid elements cannot move into regions of different
E and ∇p within
a collision time**, the **convective derivative dv/dt effectively
vanishes**, leading to:

```
    - **Electromagnetic term (enE)** → Governs charged particle movement
    - **Thermal term (KT∇n)** → Determines temperature-driven spread
    - **Balancing both effects** → Controls overall plasma behavior


    ---


    ### **Experimental Techniques to Measure Mobility & Diffusion**
    Scientists use various methods to evaluate plasma transport coefficients:
    1. **Langmuir Probes** → Measure plasma electron density & temperature
    2. **Laser-Induced Fluorescence** → Tracks ion velocity distributions
    3. **Electromagnetic Interferometers** → Detect charge density
    fluctuations
    4. **Magnetically Confined Plasma Tests** → Observe charged particle drift


    ---


    ### **Real-World Plasma Applications**
    - **Spacecraft Propulsion** → Ion thrusters rely on precise mobility
    control
    - **Astrophysical Plasmas** → Understanding interstellar gas behavior
    - **Fusion Plasma Confinement** → Magnetic fields regulate charged species
    diffusion
    - **Advanced Materials Processing** → Plasma etching in semiconductor
    industries


    Plasma transport dynamics play a **critical role in aerospace,
    astrophysics, and energy research**.
    By optimizing **mobility and diffusion**, engineers improve plasma
    confinement, propulsion efficiency,
    and material interactions.
```

Nonmetal or metal fiber-reinforced copper or copper alloy matrix composites not only retain the high electrical conductivity and high thermal conductivity of copper, but also exhibit high strength and high-temperature resistance. For example, carbon fiber-reinforced copper matrix composites combine the advantages of carbon fibers, such as self-lubrication, wear resistance, and a low thermal expansion coefficient, with the advantages of copper, such as good conductivity and thermal conductivity; consequently greatly extend the material service life; and enhance its reliability. Carbon fiber-reinforced copper matrix composites are not only used in sliding electrical contact materials, brushes, power semiconductor support electrodes and integrated circuit radiators, but also have a number of potential applications in the load bearings of the automobile engine, and the powder metallurgy bearings of printing machinery, papermaking machinery, textile machinery, and light industrial machinery.

 The fibers used to reinforce copper alloys include carbon fibers, tungsten wires, graphite fibers, alumina fibers, carbon nanotubes, silicon carbide fibers, and steel fibers. Among these fibers, tungsten wires and

carbon fibers are the most commonly used reinforcements. Also, the addition of carbon nanotubes and buckytubes into copper alloys is conducive to the resulting composites having high strength, low thermal expansion coefficients, and thermal conductivity, and particularly improves their wear resistance. (2) Particle-reinforced copper matrix composites The preparation methods for particle-reinforced copper matrix composites are similar to those of other particle-reinforced metal matrix composites and include conventional casting, conventional powder metallurgy, the co-deposition method, and the internal oxidation method. Tungsten, molybdenum, tungsten carbide, and alumina are usually used as reinforcements because of their high-temperature hardness, high melting points, and anti-adhesion properties. Using the powder metallurgy method, the reinforcements and Cu powders are mixed and are then sintered together to form copper matrix composites.

particle-reinforced copper amorphous alloy matrix composites. For example, the nano-Al_2O_3-reinforced Cu-0.3%Al composite prepared by the internal oxidation method shows good performance and has micro-hardness of more than 1000 MPa. Zirconium carbide particle-reinforced copper amorphous alloy matrix composites exhibit tensile strengths of up to 2200 MPa.

 reinforced copper matrix composites are fabricated by the following method. By forging, drawing, or rolling a series of Cu–X alloys, the X metals form filamentous or zonal distributions along the deformation direction, and consequently form Cu–X microstructure composites. During the drawing and rolling process, the X elements are elongated under the axial force into filamentous or zonal distributions with thicknesses of less than 10 nm. The contribution of the filamentous body to the overall strength of the microstructural composites is not large, because thinning of the filamentous body can increase the phase interface and hamper dislocation movement. Cu–X microstructure composites exhibit not only ultrahigh strength (maximum tensile strength of more than 2000 MPa) and very high electric conductivity, but also good heat resistance, excellent composite microstructures, and high-preferred grain orientations. These composites can be used to produce thrusters and heat exchangers beside point welding electrodes. Compared with traditional copper alloys, the alloy elements of such composites have greater content and fewer types. The X materials include the refractory metals (W, Mo, Nb, and Ta), and other elements (e.g., Cr, Fe, V). Cu–X composites can be divided according to the X elements into two categories. 1) The X elements are refractory metals with high melting points and good heat resistance (e.g., W, Mo, Nb, Ta). As strengthening elements, the refractory metals have a good strengthening effect on the X-Cu composites. 2) Although the refractory metals exhibit good strengthening effects when acting as the strengthening phase, their cost is relatively high. In situ reinforced Cu Fe, Cu–Cr, Cu–V, and other copper matrix composites have high strength with low cost. Their strengths are also above 1000 MPa, although this strength is lower than that of the Cu–Nb category. In such microstructured composites, the Cr, Fe, and V elements with band or filamentous shapes are also distributed along the axial direction.

 Fiber-Reinforced Titanium Matrix Composites The continuous fiber reinforcements used are mainly ceramic fibers such as alumina, boron carbide, and silicon carbide, and they exhibit high melting points, good thermal stability, high specific strengths, and high specific stiffnesses. Among these ceramic fibers, both alumina and boron fibers have thermal expansion coefficients that are very close to that of the titanium matrix, but boron fibers cannot resist high temperatures and alumina fibers react very strongly with the titanium matrix, so their applications are significantly restricted. At present, carbon-coated SiC fibers are commonly used in industry. Continuous SiC fiber-reinforced TMCs offer high specific strength,

high specific stiffness, high service temperatures, and good fatigue and creep properties. For example, SCS-6 SiC/IMI834 composites developed in Germany have tensile strengths up to 2200 MPa and elastic moduli up to 220 GPa. These composites also exhibit extremely high thermal stability, and their mechanical properties are not reduced after heat exposure at 700 °C for 2000 h. Replacing compressor disks with TMC leaf joints can reduce component weight by 70%.

Particle-Reinforced Titanium Matrix Composites Reinforcements for particle-reinforced titanium matrix composites (PTMCs) include carbides such as TiC, B4C, and SiC; borides such as TiB and TiB2; metal oxides such as Al2O3, Zr2O3, and R2O3 (where R is a rare earth element); and intermetallic compounds such as Ti3A1, TiAl, and Ti5Si3. Among these particles, the most commonly used reinforcements are TiB, TiB2, and TiC. Various preparation methods can be used to fabricate particle-reinforced titanium matrix composites, and they include melt casting, powder metallurgy (PM)

Melt casting for preparation of discontinuous reinforced titanium matrix composites has excellent qualities such as a simple process, good feasibility, and low costs and offers easy preparation of complex components. However, it also has weaknesses such as the strong reactivity of both titanium and the reinforcement in the liquid phase, poor wettability between the matrix and the reinforcement and uneven reinforcement distribution. To overcome these disadvantages, in situ synthesis melt casting has been investigated. In this method, carbon, boron, and other elements are added to the molten titanium metals, or other reactive gases are input into the molten titanium metals, and they then react with the liquid titanium alloys to form in situ products such as TiC and TiB particle reinforcements. The in situ synthesis of reinforcements can overcome the poor wettability between the reinforcement and the matrix to produce a uniform reinforcement distribution and consequently enhance the titanium matrix composite performances.

Radiative recombination:

If it is a particle, the process is called three-body recombination. The loss of plasma by recombination can be represented by a negative source term in the equation of continuity. It is clear that this term will be proportional to $n_e n_i ¼ n^2$. In the absence of the diffusion terms, the equation of continuity then becomes $\partial n = \partial t ¼ \alpha n^2$ ð5:41Þ The constant of proportionality α is called the recombination coefficient and has units of m3/s. Equation (5.41) is a nonlinear equation for n. This means that the straightforward method for satisfying initial and boundary conditions by linear superposition of solutions is not available. Fortunately, Eq. (5.41) is such a simple nonlinear equation that the solution can be found by inspection. It is 1 n r;t ð Þ¼ 1 n0 r ð Þþαt.

Magnesium Matrix Composites Magnesium, which has extremely rich reserves on earth, is the lightest metallic material among the structural materials in nature, in which the density of pure magnesium is 1.74 g/cm3. Magnesium has high specific strength, high specific stiffness, good damping properties, and excellent processing performance. Therefore, magnesium and its alloys promise to become one of the most widely used metal materials in high-tech industries in the twenty-first century. However, magnesium alloy applications are restricted by their low hardness, low strength, low modulus, poor wear resistance, and high thermal expansion coefficient. Magnesium matrix composites can overcome or reduce these inadequacies of magnesium alloys; consequently, these composites also become the lightweight metal

matrix composites with the most competitive advantages after aluminum matrix composites. Magnesium matrix composites exhibit high specific stiffness and high thermal conductivity.

Density decay curves of a weakly ionized plasma under recombination and diffusion.
The rate of plasma loss by diffusion can be decreased by a magnetic field; this is the problem of confinement in controlled fusion research. Consider a weakly ionized plasma in a magnetic field (Fig. 5.10). Charged particles will move along B by diffusion and mobility according to Eq. (5.10), since B does not affect motion in the parallel direction.

Fig. 5.11 Particle drifts in a cylindrically symmetric plasma column do not lead to losses
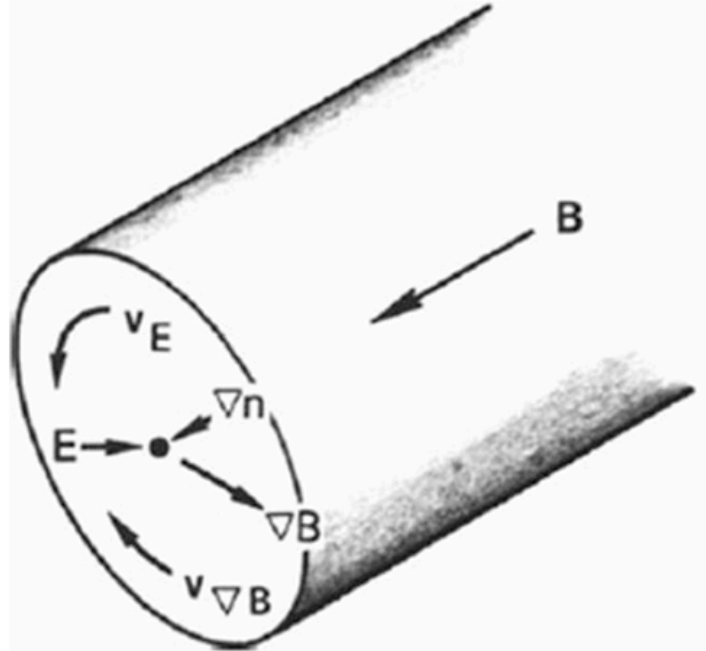
$$\Gamma_z = \pm \mu n E_z - D \frac{\partial n}{\partial z} \tag{5.44}$$

When there are collisions, particles migrate across B to the walls along the gradients. They do this by a random-walk process (Fig. 5.12). When an ion, say, collides with a neutral atom, the ion leaves the collision traveling in a different direction. It continues to gyrate about the magnetic field in the same direction, but its phase of gyration is changed discontinuously. (The Larmor radius may also change, but let us suppose that the ion does not gain or lose energy on the average.) The guiding center, therefore, shifts position in a collision and undergoes a random walk. The particles will diffuse in the direction opposite ∇n. The step length in the random walk is no longer λm, as in magnetic-field-free diffusion, but has instead the magnitude of the Larmor radius rL. Diffusion across B can therefore be slowed down by decreasing rL; that is, by increasing B.

The main continuous reinforcements for magnesium matrix composites can be divided into two categories: Al2O3 fibers and carbon (graphite) fibers. Carbon (graphite) fiber-reinforced magnesium matrix composites.

Plasma: Ambipolar Diffusion Across B Because the diffusion and mobility coefficients are anisotropic in the presence of a magnetic field, the problem of ambipolar diffusion is not as straightforward as in the B¼0case. Consider the particle fluxes perpendicular to B

 Ordinarily, since $\Gamma_{e\perp}$ is smaller than $\Gamma_{i\perp}$, a transverse electric field would be set up so as to aid electron diffusion and retard ion diffusion. However, this electric field can be short circuited by an imbalance of the fluxes along B. That is, the negative charge resulting from $\Gamma_{e\perp} < \Gamma_{i\perp}$ can be dissipated by electrons escaping along the field lines. Although the total diffusion must be ambipolar, the perpendicular part of the losses need not be ambipolar. The ions can diffuse out primarily radially, while the electrons diffuse out primarily along B. Whether or not this in fact happens depends on the particular experiment. In short plasma columns with the field lines terminating on conducting plates, one would expect the ambipolar electric field to be short-circuited out. Each species then diffuses radially at a different rate. In long, thin plasma columns terminated by insulating plates, one would expect the radial diffusion to be ambipolar.
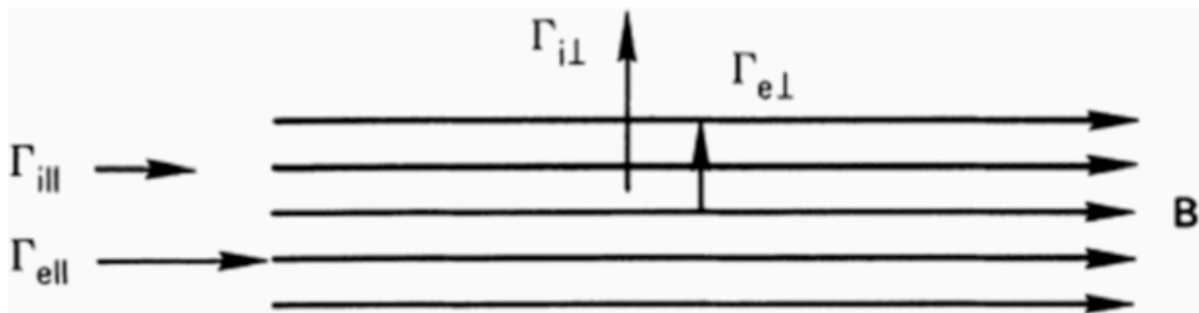

Fig. 5.13 Parallel and perpendicular particle fluxes in a magnetic field